ResearchGate

See discussions, stats, and author profiles for this publication at: https://www.researchgate.net/publication/50591084

Effect of Ortho Substitution on the Charge Localization of Dinitrobenzene Radical Anions

ARTICLE *in* THE JOURNAL OF PHYSICAL CHEMISTRY A · MARCH 2011

Impact Factor: 2.69 · DOI: 10.1021/jp200829r · Source: PubMed

CITATIONS
13

READS
36

3 AUTHORS, INCLUDING:

João Paulo Telo
Technical University of Lisbon
56 PUBLICATIONS **1,017** CITATIONS
SEE PROFILE

Stephen F Nelsen
University of Wisconsin–Madison
118 PUBLICATIONS **2,259** CITATIONS
SEE PROFILE

Available from: Stephen F Nelsen
Retrieved on: 24 January 2016

THE JOURNAL OF PHYSICAL CHEMISTRY A

ARTICLE

pubs.acs.org/JPCA

Effect of Ortho Substitution on the Charge Localization of Dinitrobenzene Radical Anions

João P. Telo,*[,†] Almaz S. Jalilov,[‡] and Stephen F. Nelsen*[,‡]

[†]Centro de Química Estrutural, Instituto Superior Técnico, Av. Rovisco Pais, 1049-001 Lisboa, Portugal

[‡]Department of Chemistry, University of Wisconsin, 1101 University Avenue, Madison Wisconsin 53706-1396, United States

Supporting Information

ABSTRACT: Optical and electron paramagnetic resonance spectroscopies were used to study the radical anions of several *m*-dinitrobenzenes and *p*-dinitrobenzenes with substituents on ortho positions relative to the nitro groups. 1,4-Dinitrobenzene, 1,4-dimethyl-2,5-dinitrobenzene, and 2,5-dinitrobenzene-1,4-diamine radical anions are delocalized (class III) mixed valence species, but in the dinitrodurene radical anion the nitro groups are forced out of the ring plane due to the steric hindrance, which results in localization of the charge. The radical anions *m*-dinitrobenzene, 2,6-dinitrotoluene, and dinitromesitylene are all localized (class II) mixed valence species, as is common for *m*-dinitrobenzenes, and the rate of intramolecular electron transfer reaction strongly decreases with the number of methyl substituents. The same mechanism of rotation of the nitro groups out of the ring plane due to steric hindrance caused by neighboring methyl groups is also responsible for slowing the reaction. However, 2,6-dinitroaniline radical anion and 2,6-dinitrophenoxide radical dianion are charge-delocalized because the strong electron releasing amino and oxido groups increase the conjugation between the two charge-bearing units.

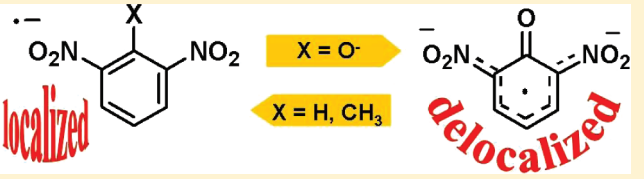

INTRODUCTION

Mixed valence (MV) systems have often been used as simple models to understand basic aspects of electron transfer.[1] Such knowledge can have possible use in molecular electronics, where the understanding of electron transport at a single-molecule scale in molecular or nanodevices is essential for controlling conductance through molecular wires.[2] The simplest MV compounds have two charge-bearing units (CBUs) **M** symmetrically connected by a bridge **B** and have an odd overall charge, so that the two **M** units may be at different redox levels. According to the Robin and Day classification,[3] class II (localized) MV compounds are described as two charge-localized structures in equilibrium, $\mathbf{M}^0-\mathbf{B}-\mathbf{M}^{-1} \leftrightarrows \mathbf{M}^{-1}-\mathbf{B}-\mathbf{M}^0$. Each of these charge-localized structures corresponds to a minimum in the adiabatic potential surface of the ground state (see Figure 1) and the two interconvert through the thermally activated electron transfer between **M** units. Class III (delocalized) MV compounds have instantaneously the same fractional charge at the two **M** units and, in the case of having a single negative overall charge, can be described as $\mathbf{M}^{-1/2}-\mathbf{B}-\mathbf{M}^{-1/2}$, although significant charge is also present on the bridge. In the Marcus−Hush two state model,[4] the adiabatic potential surfaces are parabolic and depend only on two parameters: the reorganization energy λ, and the electronic coupling between the charge-bearing units H_{ab}. The class II double-minimum ground state surface occurs for systems with $\lambda > 2H_{ab}$. At $\lambda = 2H_{ab}$ the two minima merge into a single one at the II/III borderline and for $\lambda < 2H_{ab}$ the system is charge-delocalized (class III, Figure 1). Both λ and H_{ab} can be obtained from the intervalence charge-transfer band (ICTB), which is normally the lowest-energy band in the near-infrared part of the compound's optical spectrum. Localized and delocalized MV compounds can be distinguished by their ICTBs for the dinitroaromatic radical anions that we discuss here. Class III compounds show narrow ICTBs, with vibrational structure,

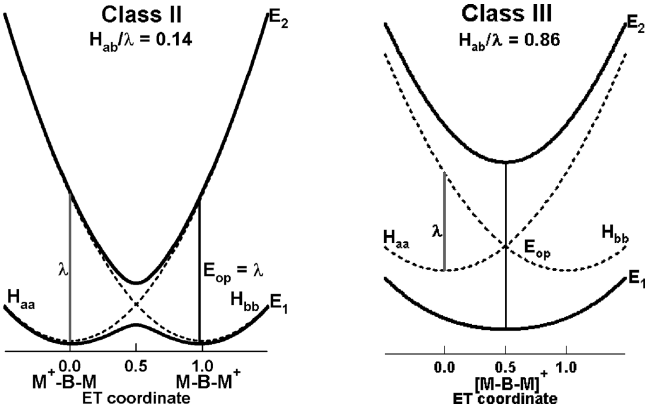

Figure 1. Marcus−Hush diagrams for localized (class II) and delocalized (class III) mixed-valence compounds, shown using the frequently applied single two-state model.

Received: January 26, 2011
Revised: February 28, 2011
Published: March 18, 2011

ACS Publications © 2011 American Chemical Society

Chart 1. Structures of Cryptand[2.2.2] and *p*-Dinitrobenzenes (upper row) and *m*-Dinitrobenzenes (lower row) Derivatives Discussed in This Work

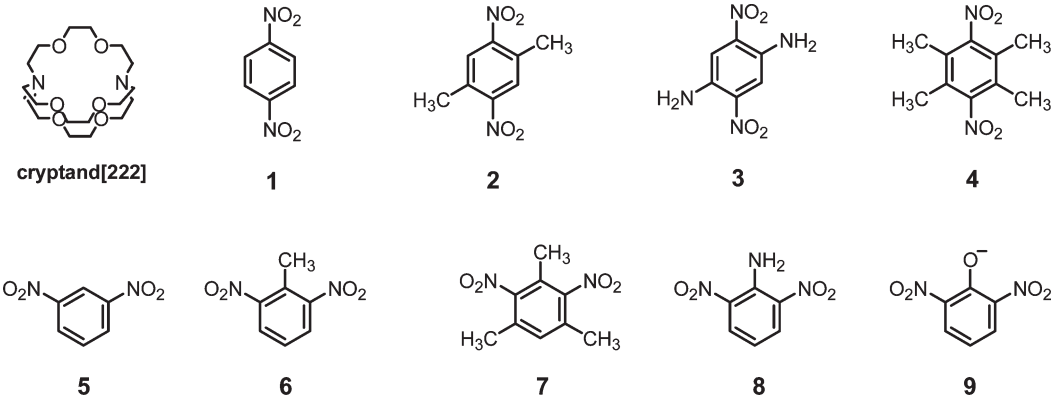

while class II compounds show much broader and featureless Gaussian-shaped bands.

Symmetrical dinitroaromatic radical anions were among the first organic MV compounds for which intramolecular electron transfer (IET) reactions were studied by electron paramagnetic resonance (EPR) spectroscopy.[5] However, these systems were not discussed as MV systems because this concept was only developed in the later 1960s for transition-metal coordination compounds by Robin and Day[3] and Hush.[4c] The electronic structure of *p*-dinitrobenzene (**1**) radical anion (Chart 1) in aprotic solvents was always found to be delocalized on the two nitro groups,[6] but its tetramethyl derivative, dinitrodurene (**4**) radical anion, was one of the first radicals for which IET was ever detected by EPR spectroscopy.[5d] It was assumed that $\mathbf{4}^-$ exists as an equilibrium between two forms, each having alternately one of the nitro groups out of the plane of the molecule, thus providing a mechanism for the modulation of the nitrogen coupling constants. In the case of radical anions of *m*-dinitrobenzene derivatives, the non-Kekule substitution pattern of the nitro groups induces a low electronic coupling, leading to charge localization, as shown by EPR spectroscopy.[5c,e,7] Hydrogen bonding of the reduced nitro group to the solvent increases the reorganization energy λ, so that the rate of IET of $\mathbf{5}^-$ in alcohols or water is reduced by several orders of magnitude as compared to the one in aprotic solvents.[7a] However, the rate of the reaction on 2,6-dinitrophenoxide radical dianion $\mathbf{9}^-$ in basic aqueous solution is unusually fast for a *m*-dinitrobenzene derivative. It is more than 4 orders of magnitude faster than in 2,6-dinitrophenol radical anion, its protonated form obtained at neutral aqueous solutions.[8]

These disparities led us to analyze more systematically the effect of ortho substitution on the class II/III nature of radical anions from *p*-dinitrobenzene (**1**−**4**) and *m*-dinitrobenzene (**5**−**9**) derivatives prepared in the presence of cryptand[2.2.2], not only by EPR but also by the more revealing optical spectroscopy.

EXPERIMENTAL PART

p-Dinitrobenzene (**1**) and *m*-dinitrobenzene (**5**) were purchased from Aldrich and recrystallized before use. Line superposition in the EPR spectra of $\mathbf{5}^-$ strongly decreases the accuracy of the simulations, so the EPR spectra of $\mathbf{5}^-$ was done with the perdeuterated compound obtained by double nitration of benzene-d_6. The remaining dinitrobenzene derivatives were prepared according to known procedures and purified by column chromatography, followed by recrystallization. 2,6-Dinitrophenol (from Aldrich) was dissolved in ethanol, and a warm alcoholic NaOH solution added until no further precipitation occurred. 2,6-Dinitrophenoxide (**9**) was then filtered and washed with ethanol.

The radical anions were prepared in vacuum-sealed glass cells equipped with an EPR tube and a quartz optical cell. Reduction was achieved by contact with 0.2% Na−Hg amalgam. The nitro compound, an excess of commercial cryptand[2.2.2] to sequester the sodium cation, and the Na−Hg amalgam were introduced in different chambers of the cell under nitrogen. The cryptand was degassed by melting under high vacuum before addition of the solvent. The concentration of the samples was determined spectrophotometrically before reduction.

The rate constants for the intramolecular ET reaction were obtained by simulating the experimental ESR spectra. The simulation program solves the Bloch equations for a two-state model. Asymmetric line broadening was included in the simulations by making the intrinsic line width Γ of each line dependent on its nitrogen quantum number $\overline{m}$, according to the empirical equation $\Gamma(\overline{m}) = A + B\overline{m} + C\overline{m}^2$.[9]

RESULTS AND DISCUSSION

a. *p*-Dinitrobenzene Derivatives. The optical spectrum of *p*-dinitrobenzene radical anion $\mathbf{1}^-$ in MeCN (Figure 2) has a narrow low-energy optical band with vibrational structure, showing that it is a delocalized MV compound.[6] Double substitution of hydrogen by methyl in $\mathbf{2}^-$ or amino groups ($\mathbf{3}^-$) has a minor effect on the position or shape of the low-energy delocalized band. The optical band in $\mathbf{3}^-$ is less intense and shifted to lower energies by 570 cm^{-1}. This radical also shows an extra band at intermediate energies (14940 cm^{-1}). As is common for delocalized optical bands, changing solvent has a small effect on the maximum of the band. Spectra of the three radical anions in DMF show a negligible shift of the low energy band maximum compared to MeCN (spectra not shown).

Contrary to the previous examples, the radical anion of the tetramethyl dervative dinitrodurene $\mathbf{4}^-$ shows a broad and featureless band typical of a localized radical (Figure 3) with a maximum at λ=10300 cm^{-1}. Localization occurs because the

dx.doi.org/10.1021/jp200829r |*J. Phys. Chem. A* 2011, 115, 3016–3021

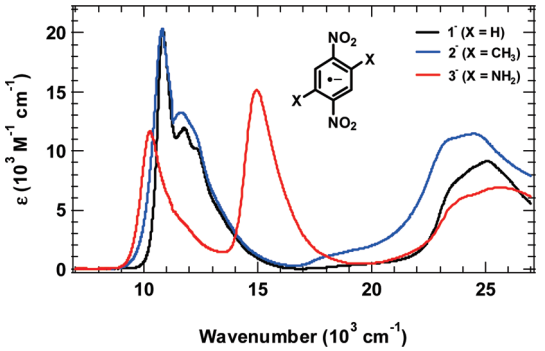

Figure 2. Optical spectra of $\mathbf{1}^-$, $\mathbf{2}^-$, and $\mathbf{3}^-$ in MeCN.

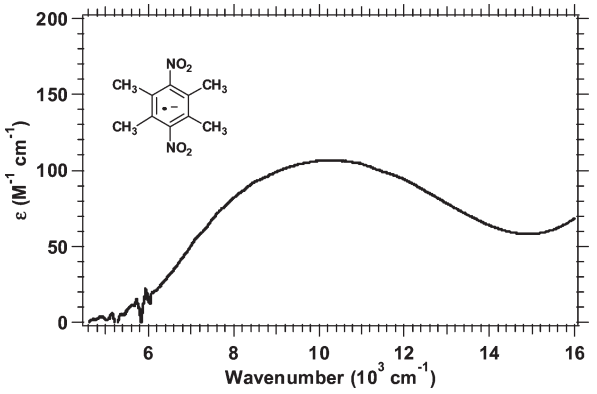

Figure 3. Optical spectrum of $\mathbf{4}^-$ in MeCN.

Table 1. Rate Constants and Eyring Parameters for IET Reaction Extracted from EPR Spectra in MeCN

	4^-	5^{-b}	6^-	7^-
$k(298)$, 10^8 s^{-1a}	154 (±76)	164 (±42)	41 (±26)	~5
$\Delta H^{\ddagger}$ (kcal/mol)	2.6 (±0.13)	2.86 (±0.07)	3.7 (±0.19)	5[d]
$\Delta S^{\ddagger}$ (cal/(mol·K))	−3.1 (±0.5)	−2.2 (±0.3)	−2.1 (±0.3)	−0.4[d]
T range (K)	230−310	226−285[c]	250−330	320, 298, 240[d]

[a] Obtained by interpolation of the Eyring plot (extrapolation in the case of $\mathbf{5}^-$). [b] EPR done with the perdeuterated compound. Hosoi and Masuda[10] report $k_{(298)}$ = 463 × 10^8 s^{-1}. [c] Spectra in the fast limit above 285 K. [d] Three points only. Spectra too close to the slow limit to provide more accurate data.

steric interaction with the methyl groups forces the nitros out of the molecule plane. The radical anion most stable conformation calculated using UHF/6-31+G(d) has a charge-localized structure with C−N distances of 1.399 and 1.470 Å, and very different NO_2 twist angles of 45.0° at the reduced NO_2 group and 70.0° at the nearly neutral one. Interconversion between the two charge-localized structures provides the exchange of the main charge density between the two CBUs.

EPR spectroscopy confirms this different behavior. Radicals $\mathbf{1}^-$−$\mathbf{3}^-$ show EPR spectra with an average coupling constant for the two nitrogen atoms and no evidence of alternating line broadening effects (see Supporting Information for EPR data). On the contrary, the EPR spectra of $\mathbf{4}^-$ in MeCN show clear evidence of temperature-dependent alternating line broadening effects on the nitrogen quintet (Figure S2, Supporting Information). Simulation

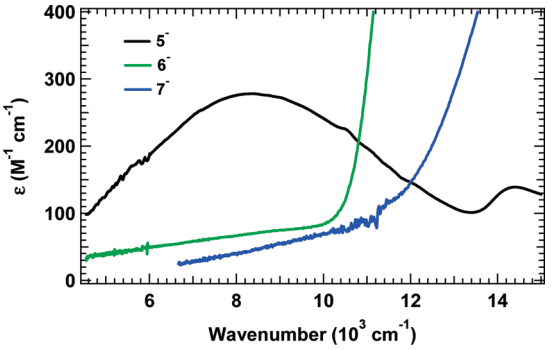

Figure 4. Optical spectra of *m*-dinitrobenzene (**5**), 2,6-dinitrotoluene (**6**), and dinitromesytilene (**7**) radical anions in MeCN.

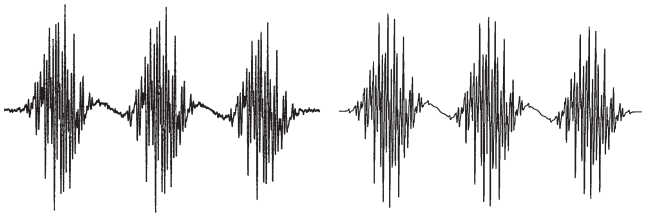

Figure 5. Experimental EPR spectra of dinitromesitylene radical anion $\mathbf{7}^-$ at 298 K in MeCN (left-hand side) and computer simulation with k = 5 × 10^8 s^{-1} (right-hand side).

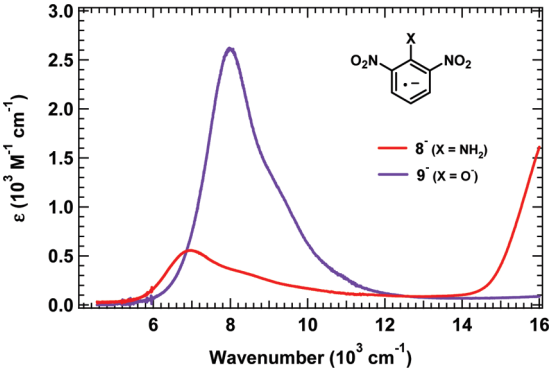

Figure 6. Optical spectra of 2,6-dinitroaniline radical anion ($\mathbf{8}^-$) and 2,6-dinitrophenoxide radical dianion ($\mathbf{9}^-$) in MeCN.

of the spectra at different temperatures afforded the rate of IET and Eyring parameters found in Table 1.

b. *m*-Dinitrobenzene Derivatives. Figure 4 compares the low energy portion of the optical spectra of the radical anions of compounds **5**−**7**. The non-Kekule substitution pattern of *m*-dinitrobenzene radical anion $\mathbf{5}^-$ induces a small electronic coupling between nitro groups, so its optical spectrum shows the typical wide and Gaussian shaped band of the charge-localized (class II) compounds with an energy maximum (which equals the reorganization energy λ in the Marcus−Hush model) of 8400 cm^{-1} (ε_{max} = 280 M^{-1} cm^{-1}). The 2-methyl-substituted radical anion $\mathbf{6}^-$ has a much less intense CT band, partially hidden by higher energy bands. The maximum of the band is not visible but occurs clearly at wavenumbers higher than 10000 cm^{-1}. The decrease in intensity and increase of λ_{max} are even more pronounced in $\mathbf{7}^-$. According to Hush theory, the

dx.doi.org/10.1021/jp200829r |J. Phys. Chem. A 2011, 115, 3016–3021

Chart 2. Canonical Forms of 2,6-Dinitrophenoxide (9) and Delocalized Structure of Radical Dianion 9^-

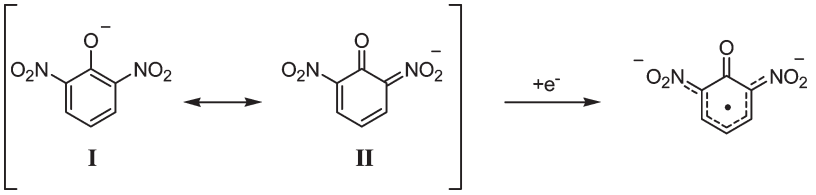

electronic coupling H_{ab} of class II compounds is proportional to the intensity of its ICTB.[4c,d] As in dinitrodurene radical anion, rotation of the nitro groups out of the benzene plane due to steric interaction with the methyl groups decreases the electronic coupling between the CBUs, decreasing the intensity of the band. This is accompanied with an increase of charge and spin density on the nitro groups, as can be seen by the increase of the average nitrogen coupling constant, which in MeCN at room temperature changes from 4.2 G in $\mathbf{5}^-$ to 4.7 G in $\mathbf{6}^-$ and 7.0 G in $\mathbf{7}^-$. Since in a class II radical the negative charge is instantaneously concentrated in one of the CBUs, this increase in charge makes the reduced and unreduced nitro groups more different, resulting in a higher λ value.

The EPR spectra also reveal this increase in λ/H_{ab} ratio. According to the Marcus−Hush two-stage model, the barrier height of the IET reaction is given by $\Delta G^* = \lambda/4 - H_{ab} + (H_{ab})^2/\lambda$, so the activation energy of the reaction should increase from $\mathbf{5}^-$ to $\mathbf{7}^-$. As can be seen in Table 1, the rate of the reaction decreases 4-fold from $\mathbf{5}^-$ to $\mathbf{6}^-$, mostly due to the increase in the activation enthalpy. From $\mathbf{6}^-$ to $\mathbf{7}^-$ the rate constant is reduced by a factor of 8, but the EPR spectra of $\mathbf{7}^-$ are so close to the slow limit that an accurate measurement of the rate at different temperatures is difficult. As can be seen in Figure 5, the spectrum of $\mathbf{7}^-$ at room temperature shows mostly three groups of lines corresponding to one nitrogen coupling constant. The only hint of the remaining two $\overline{m} = \pm 1$ lines of the nitrogen quintet is the waving of baseline between main groups of lines. This effect is more intense at 320 K and gradually disappears, lowering the temperature. This allowed simulations at three temperatures and a rough estimation of the activation parameters. We discussed calculations on $\mathbf{5}^-$ previously.[6a] UHF/6-31+G(d) calculations on $\mathbf{6}^-$ gave twists at the reduced nitro group of 8.4° and at the nearly neutral one of 48.9°, and for $\mathbf{7}^-$ a 33.8° twist angle at the reduced nitro group and 68.9° at the nearly neutral one.

The low-energy bands of the radical anions from **8** and **9** are shown in Figure 6. Both $\mathbf{8}^-$ and $\mathbf{9}^-$ show narrower and more intense bands than the radicals of Figure 4, with maxima at 6960 cm^{-1} (ε = 555 M^{-1} cm^{-1}) and 7990 cm^{-1} (ε = 2610 M^{-1} cm^{-1}), respectively. They seem to show partially resolved vibrational structure, suggesting they are class III delocalized mixed-valence compounds. The EPR spectra of $\mathbf{8}^-$ and $\mathbf{9}^-$ confirm this assumption. Both show an average coupling constant for the two nitro group nitrogens and no broadening effects due to IET. The reason for this unusual behavior of a meta-substituted dinitrobenzene radical anion lies in the strongly electron donating properties of the amino and oxido groups.

We suggest that resonance forms from the electron-donating group in position 2 contribute to the increased conjugation between nitro groups, and the effect is obviously higher in the phenolate dianion than in the aniline. As shown in the canonical forms of Chart 2, there are formal structures like **II** where the

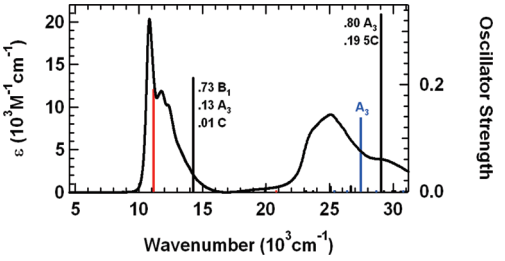

Figure 7. Comparison of the optical spectrum of 1,4-dinitrobenzene radical anion ($\mathbf{1}^-$) in acetonitrile with the TD-DFT (black sticks with fractional contributions shown) and Koopmans based calculations (colored sticks).

delocalization of the oxido group charge into the nitro groups results in an increase of the conjugation between CBUs. The importance the of structure **II** contribution can be found in the interatomic distances determined by X-ray diffraction studies on crystals of potassium 2,6-dinitrophenolate. The C1−C2 and the C6−C1 bonds (d = 1.452 Å) are the longest bonds found in benzenoid rings. In contrast, the other C−C bonds (average d = 1.385 Å) are shorter than the typical bonds in benzene (d = 1.395 Å).[11]

The same happens with the calculated distances in the radical dianion $\mathbf{9}^-$ using UB3LYP/6-31+G(d), where $d_{C1C2} = d_{C1C6}$ = 1.497 Å and the remaining C−C bonds average 1.407 Å. Moreover, the C1−O bond is calculated to be 1.239 Å, closer to a carbonyl double bond (1.21−1.22 Å) than to the C−O bond in phenoxides (1.31−1.33 Å).[12] Interestingly, contrary to the previous *m*-dinitrobenzene derivatives $\mathbf{5}^-$ to $\mathbf{7}^-$, structure optimization of $\mathbf{9}^-$ with UHF/6-31+G(d) always yields a charge-delocalized structure with bond lengths very similar to the DFT ones.

Comparison of TD-DFT with Koopmans-Based Calculations of Optical Spectra. We consider here how well the TD-DFT and Koopmans-based calculations for the compounds showing charge-delocalized radical anions fit the observed optical spectra. $\mathbf{6}^-$ has a charge-localized structure with most of its charge on one nitro group, which causes it to have a broad Hush-type nearly Gaussian class II charge transfer band. The B3LYP calculations used for delocalized compounds also delocalize the charge in these radical anions, so the actual structures for $\mathbf{4}^-$ to $\mathbf{7}^-$ are very different from the calculated ones, and as expected, their experimental spectra are very different from those that are calculated for delocalized species. The other compounds have the spectra expected for delocalized (class III) mixed valence compounds, and we examine here how well their spectra are calculated.

The plots in Figures 7, 8, and 9 show TD-DFT calculations as black sticks and include the assignments of the configuration interaction for the transitions, shown using the nomenclature of

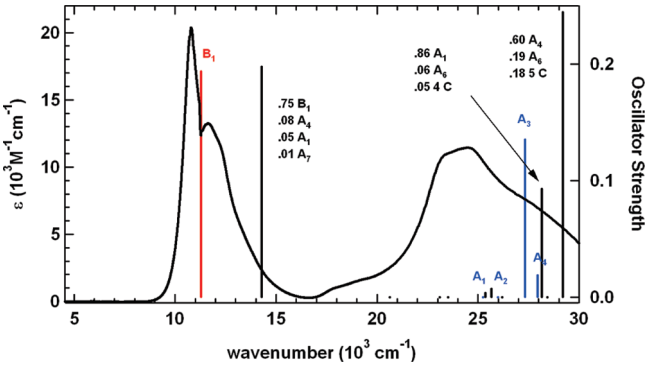

Figure 8. Comparison of the optical spectrum of 1,4-dinitro-2,5-dimethylbenzene radical anion ($\mathbf{2}^-$) in acetonitrile with the TD-DFT (black sticks with fractional contributions shown) and Koopmans based calculations (colored sticks, red for type B, blue for type A transitions).

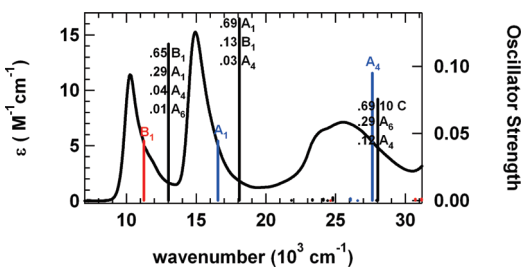

Figure 9. Comparison of the optical spectrum of 1,4-diamino-2,5-dinitrobenzene radical anion ($\mathbf{3}^-$) in acetonitrile with the TD-DFT (black sticks with fractional contributions shown) and Koopmans based calculations (colored sticks, red for type B, blue for type A transitions).

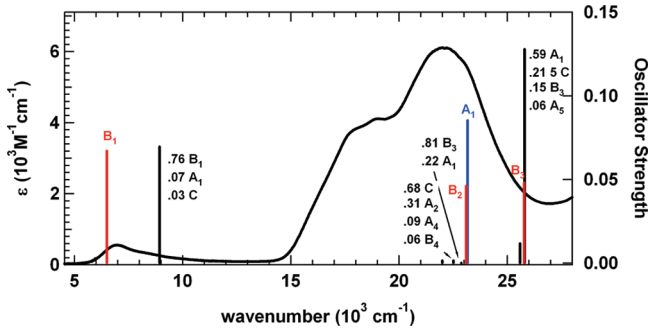

Figure 10. Comparison of the optical spectrum of 2,5-dinitroaniline radical anion ($\mathbf{8}^-$) in acetonitrile with the TD-DFT (black sticks with fractional contributions shown) and Koopmans based calculations (colored sticks).

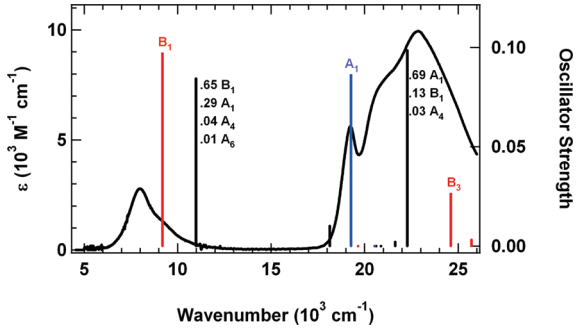

Figure 11. Comparison of the optical spectrum of 2,5-dinitrophenoxide radical dianion ($\mathbf{9}^{2-}$) in acetonitrile with the TD-DFT (black sticks with fractional contributions shown) and Koopmans-based calculations (colored sticks).

Koopmans-based transitions, which is more transparent than that used for TD-DFT calculations, which only refer to molecular orbital numbers, which are in principle different for each compound. Koopmans-based calculations are shown as red sticks for type B (from SOMO α to virtual α MOs) and blue sticks for type A transitions (from "filled" β to SOMO β MOs), which come at higher energy for these radical anions. Both are numbered in order of increasing difference between the SOMO energy and the transition energy. Koopmans-based calculations only consider these two types of transitions (all others are "type C"), which dominate the low energy transitions for the optical spectra of most radical ions. Both the calculations were carried out at the same level, using geometry optimized B3LYP/6-31G(d) structures. Koopmans-based calculations are carried out at the optimized geometry of the radical ion, doing single point calculations of the neutral in radical anion geometry for the type B transitions and the dianion in radical anion geometry for type A for these radical anions. This artificially empties the SOMO for the type B transitions, so the same number of electrons (zero) is in the orbitals whose energies are compared. Type B transition energies are given by the energy gap between what was the SOMO in the radical anion and each virtual orbital. The dianion used for the type A transitions fills the SOMO, so there are two electrons in each orbital whose energies are compared for the type A transitions. Transition energies for type A transitions are given by the energy gap between each filled orbital and what was the SOMO in the radical anion. The fact that the type B transition energy calculations work at least as well as those for the type A MOs that Koopmans' theorem addressed, despite the fact that orbital occupancy is tiny for virtual MOs so that the virtual MO energies are nearly unoptimized during the geometry optimization procedure seems surprising. It emphasizes that the problem with calculating transition energies for optical absorptions is principally related to comparing the energies of MOs with different occupancy (in the absence of large configuration interaction effects) and that configuration interaction is not very important for many radical ions. Configuration interaction is very important for typical closed-shell systems. Although configuration interaction should only lower transition energies, the Koopmans-based calculations for these compounds give lower energy transitions than do the TD-DFT calculations, and that the calculated transition energies are all overestimated, so agreement with experiment is better for the Koopmans-based calculations than for the TD-DFT calculations. It is only appropriate to use Koopmans-based calculations for lower energy transitions, because the type C transitions that it ignores become increasingly important at higher energy.

a. *p*-Dinitrobenzene Derivatives. Although $\mathbf{1}^-$ and $\mathbf{2}^-$ give rather similar oscillator strength estimates by TD-DFT and Koopmans-based methods, those obtained for $\mathbf{3}^-$ are about a factor of 2 smaller for the B_1 and A_1 Koopmans-based calculations, and although bands of more comparable intensity are calculated to occur at nearly the same energy by the two methods near 28000 cm^{-1}, it is assigned by TD-DFT to be dominated by type C transitions that the Koopmans-based calculations ignore, and only to have a small contribution from the A_4 band to which

Chart 3. 2,6-Disubstituted Phenol as a pH-Controlled Switch

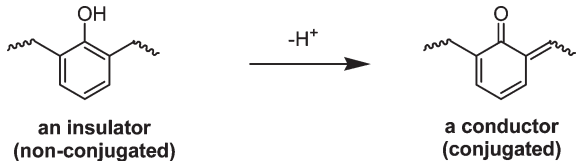

the Koopmans-based calculation assigns most of the intensity contribution for the transition. We conclude that there are likely to be some type C bands contributing to the broad absorption in the >23000 cm^{-1} region, although TD-DFT does not seem to do a much better job of predicting this region than do Koopmans-based calculations; neither method does very well.

b. *m*-Dinitrobenzene Derivatives. Figures 10 and 11 compare the optical spectra of the delocalized *m*-dinitrobenzene derivatives studied. Both calculations overestimate the relative intensity of the lowest energy (B_1) band relative to the higher energy absorption region. The Koopmans-based calculations predict the energy of the bands better than do the TD-DFT calculations.

CONCLUSIONS

The localized or delocalized character of ortho-substituted dinitrobenzene radical anions depends upon the nature of the substituents. Unsubstituted *p*-dinitrobenzene radical anion and their dimethyl- and diamino-substituted derivatives are all delocalized mixed valence species, but in the permethylated dinitrodurene radical anion ($\mathbf{4}^-$) the steric hindrance is enough to force the nitro groups out of the ring plane and induce localization of the charge. Radical anions $\mathbf{5}^-$, $\mathbf{6}^-$, and $\mathbf{7}^-$ are all localized mixed valence species, as is common for *m*-dinitrobenzenes, but the rate of IET reaction strongly decreases with the number of methyl substituents. The same mechanism of rotation of the nitro groups out of the ring plane due to steric hindrance by neighboring methyl groups is also responsible for the slowing the IET reaction. However, with strongly enough electron releasing substituents, NH_2 in $\mathbf{8}^-$ and O^- in $\mathbf{9}^-$ these systems become charge-delocalized. The effect is stronger with the strongest electron-releasing group, O^-, and the results suggest that 2,6-disubstituted phenol can act as a pH-controlled switch. If intercalated in a molecular wire through these positions, the phenol unit acts as an insulator in neutral or acid pH, because the positions 2 and 6 are not conjugated (non-Kekule). However, at basic pH deprotonation and delocalization of the negative charge affords conjugation between positions 2 and 6 and the molecule can behave as a conductor (Chart 3)

ASSOCIATED CONTENT

Supporting Information. EPR spectra, rate constants, hyperfine splittings, intrinsic line width parameters, and Eyring plots for radicals $\mathbf{2}^-$–$\mathbf{9}^-$, as well as *xyz* coordinates for the calculations discussed here. This material is available free of charge via the Internet at http://pubs.acs.org.

AUTHOR INFORMATION

Corresponding Author
*E-mail: jptelo@ist.utl.pt and nelsen@chem.wisc.edu.

ACKNOWLEDGMENT

We thank the National Science Foundation for support of this work under CHE-0647719 (SFN) and Fundação Para a Ciência e Tecnologia through its Centro de Química Estrutural and Project PTDC/QUI-QUI/101433/2008 (JPT).

REFERENCES

(1) (a) Brunschwig, B. S.; Creutz, C.; Sutin, N. *Chem. Soc. Rev.* **2002**, *31*, 168. (b) Demadis, K. D.; Hartshorn, C. M.; Meyer, T. M. *Chem. Rev.* **2001**, *101*, 2655. (c) Nelsen, S. F. *Chem.—Eur. J.* **2000**, *6*, 581.

(2) (a) Reichert, J.; Ochs, R.; Beckmann, D.; Weber, H. B.; Mayor, M.; von Lohneysen, H. *Phys. Rev. Lett.* **2002**, *88*, 176804. (b) Cui, X. D.; Primak, A.; Zarate, X.; Tomfohr, J.; Sankey, O. F.; Moore, A. L.; Moore, T. A.; Gust, D.; Harris, G.; Lindsay, S. M. *Science* **2001**, *294*, 571. (c) Nitzan, A.; Ratner, M. A. *Science* **2003**, *300*, 1384.

(3) Robin, M.; Day, P. *Adv. Inorg. Chem. Radiochem.* **1967**, *10*, 247.

(4) (a) Marcus, R. A. *J. Chem. Phys.* **1956**, *24*, 966. (b) Marcus, R. A.; Sutin, N. *Biochim. Biophys. Acta* **1985**, *811*, 265. (c) Hush, N. S. *Prog. Inorg. Chem.* **1967**, *8*, 391. (d) Hush, N. S. *Coord. Chem. Rev.* **1985**, *64*, 135.

(5) (a) Maki, A. H.; Geske, D. H. *J. Chem. Phys.* **1960**, *33*, 825. (b) Maki, A. H.; Geske, D. H. *J. Am. Chem. Soc.* **1961**, *83*, 1852. (c) Freed, J. H.; Rieger, P. H.; Fraenkel, G. K. *J. Chem. Phys.* **1962**, *37*, 1881. (d) Freed, J. H.; Fraenkel, G. K. *J. Chem. Phys.* **1962**, *37*, 11566. (e) Rieger, P. H.; Fraenkel, G. K. *J. Chem. Phys.* **1963**, *39*, 609. (f) Harriman, J. E.; Maki, A. H. *J. Chem. Phys.* **1963**, *39*, 778. (g) Freed, J. H.; Fraenkel, G. K. *J. Chem. Phys.* **1964**, *41*, 699. (h) Geske, D. H.; Ragle, J. L.; Bambenek, M. A.; Balch, A. L. *J. Am. Chem. Soc.* **1964**, *86*, 987. (e) Blandamer, M. J.; Gough, T. E.; Gross, J. M.; Symons, M. C. R. *J. Chem. Soc.* **1964**, 536.

(6) (a) Nelsen, S. F.; Konradsson, A. E.; Weaver, M. N.; Telo, J. P. *J. Am. Chem. Soc.* **2003**, *125*, 12493. (b) Nelsen, S. F.; Weaver, M. N.; Zink, J. I.; Telo, J. P. *J. Am. Chem. Soc.* **2005**, *127*, 10611.

(7) (a) Grampp, G; Shohoji, M. C. B. L.; Herold, B. J. *Ber. Bunsen-Ges. Phys. Chem.* **1989**, *93*, 58. (b) Grampp, G; Shohoji, M. C. B. L.; Herold, B. J.; Steenken, S. *Ber. Bunsen-Ges. Phys. Chem* **1990**, *94*, 1507. (c) Telo, J. P.; Grampp, G; Shohoji, M.C.B.L *Phys. Chem. Chem. Phys.* **1999**, *1*, 99.

(8) Telo, J. P.; Shohoji, M. C. B. L. *J. Chem. Soc., Perkin Trans. 2* **1998**, 711.

(9) Fraenkel, G. K. *J. Phys. Chem.* **1967**, *71*, 139 see eq 3.26, p 157.

(10) (a) Hosoi, H; Mori, Y.; Masuda, Y. 1998, 177. (b) Hosoi, H.; Masuda, Y. *J. Mol. Liq.* **2001**, *90*, 279.

(11) Andersen, E. K; Andersen, I. G. K.; Sørensen, G. P. *Acta Chem. Scand.* **1989**, *43*, 624.

(12) van der Schaaf, P. A.; Jastrzebski, J. T. B. H.; Hogerheide, M. P.; Smeets, W. J. J.; Spek, A. L.; Boersma, J.; van Koten'tt, G. *Inorg. Chem.* **1993**, *32*, 4111.